CONFERENCE PRE-PRINT

INVESTIGATION OF PLASMA-WALL INTERACTION AND IMPURITY TRANSPORT BEHAVIORS OF HL-3 PLASMAS

L. Liu*, K. Zhang, D.L. Yu, J.M. Gao, Y.L. Zhou, M.K. Han, W.J. Chen, Y.L. Wei, X.X. He, S.Q. Wang, S.S.

Yang, G.L. Xiao and Z.B. Shi Southwestern Institute of Physics

Chengdu, China

Email: liuliang@swip.ac.cn

Abstract

Plasma-wall interaction (PWI) during steady phases and transient events such as disruptions and edge localized modes (ELMs) is a critical issue in the magnetically confined plasmas, mainly because the particles and heat fluxes from plasmas need to be controlled to prevent damage to the plasma facing components (PFCs), as well as the impact of impurity influx on the main plasma performance should be mitigated. The visible imaging system is an important tool to determine the plasma configuration and boundary variation, hot spots distribution, recycling asymmetry (particle source asymmetry), wall erosion rate and particle influx (usually with the filtered line emission), etc., because visible line radiations are mainly emitted from neutral atoms or low charge-state ions in the plasma edge where the electron temperature is relatively low and radiation intensity in the scape-off layer (SOL) reflects the strength of PWI. An extreme-wide angle view diagnostic with field of view (FOV) of 120°, allowing us to observe the inner and outer walls, the divertor region, the lower hybrid current drive (LHCD) antenna and neutral beam injection (NBI) port in the visible range, was installed on the HL-3 tokamak for safe machine operation. New insights into the physical processes in the plasma edge are gained with this diagnostic by measuring the 3D emission profiles in the main chamber as well as in the divertor region. In the paper, hot spots during the PWI induced by the bulges on the divertor graphite tiles and exposed tile edges were experimentally observed, which causes the increase of impurity influxes. Bright objects (UFOs) moving through the plasma and occasionally inducing major disruption are recorded, together with the magnetic field lines development by their luminous trajectories. The online boron powder injection from the top of vacuum vessel was implemented in order to improve the wall conditions, where the interactions between the plasma edge and puffed boron powders are observed. That the boron gathering and glowing in plasma edge probably by the impurity screening mechanism and the almost simultaneous radiation (mainly the bremsstrahlung) enhancement in the plasma center because of the impurity pollution occurs. Actually, a low recycling level and high confinement phase was concurrently achieved by the online boron powder injection. The high spatial and temporal resolution imaging capability also leads to advances in the characterization of ELMs along with their impact on PFCs. During type-I ELMs, main interaction is on the lower divertor and upper baffle, indicating the enhanced particle recycling during the ELM pulse energy deposition. Zeff during one ELM event is increased, indicating the transiently increased impurity influx because of PWI. Nonetheless, Zeff is basically decreased during the H mode period, which demonstrates the impurities are expelled from the plasma by the type-I ELMs. The more the ELMs frequency is, the more impurity is expelled from the plasma.

INTRODUCTION

Plasma-wall interaction (PWI) study is one of the hot topics in the magnetically confined fusion machines mainly because excess heat load deposition on the plasma facing components (PFCs) probably causes the PFCs damage and incontrollable impurity particle influx [1]. In International Thermonuclear Experimental Reactor (ITER), due to the ripple of the toroidal magnetic field, a fraction of energetic alpha particles may be deconfined and interact with the main chamber as a focused energetic beam inducing localized hot spots [2]. The severe 'carbon bloom' on either the divertor plates or limiters during high auxiliary heating power was reported in JET and TFTR, which is a limiting mechanism to the performance of high fusion yield plasmas because of a large amount of impurity influxes produced from the overheated 'bloom' regions [3]. There is also an increasing concern in tokamaks that transient events such as disruptions [4] and edge localized modes (ELMs) [5, 6] interacting with PFCs in the divertor region and in the main chamber could be large enough to cause material erosion or melting because of large heat flux to the wall in a short time.

The PWI control is implemented mainly by measuring parameters such as surface temperature, power flux, material erosion/deposition rate, dust formation, fuel retention, etc., for steady state operation [7, 8]. The imaging method especially the infrared/visible viewing is intuitive for the PWI investigation [9, 10], e.g., the infrared (IR) thermography provides the surface temperature and power flux measurements on PFCs while the visible (VIR) imaging system measures hot spots distribution as well as the wall erosion rates and impurity influxes. Usually, several VIR/IR cameras are equipped to monitor the wall with a large area. In Tore Supra, a set of seven actively cooled infrared endoscopes were equally spaced around the torus to cover the entire surface of the toroidal pumped limiter and all heating antennae, which has significantly improved the knowledge of heat load deposition and been implemented in a feedback control system [11]. In W7-X, ten IR/visible viewing systems as part of the machine protection system were required for real time monitoring of ten discrete, water cooled divertor modules, in order to prevent local overheating of the target tiles which could easily lead to their destruction [12]. In Alcator C-Mod,

several localized regions of increased brightness associated with hot spots are measured by the visible imaging system and interpreted as heating due to localized density peaking during LHCD operation [13]. A wide-angle infrared thermography and visible observation diagnostic was designed on JT-60SA, in order to image a large section inside the vacuum vessel [14]. In JET it is reported that the toroidal asymmetry in the interaction pattern appears during the plasma disruption by two views (infrared and visible view respectively) from opposite sides of the torus [15]. Afterwards more than 25 cameras were routinely used for imaging in JET in the infrared and visible wavelength regions, whose application ranges from the protection of the JET ITER-like wall to detailed investigations of plasma—wall interactions and various instabilities [16].

In order to image a large section of the plasma and vacuum vessel both in poloidal and toroidal directions, an extreme wide-angle visible imaging system with a FOV of 120° has been installed on HL-3 tokamak, which permits observation of PWI in the main chamber and in the divertor region. In Sec. I, the experimental setup is introduced. In Sec. II, the PWI phenomena such as the hot spots distribution on the first wall, the UFOs, the boron powder injection process, and the transient events such as disruption and ELMs interacting with PFCs are characterized by the high spatial and temporal resolution diagnostic, and the impurity transport behaviours are discussed. The paper is summarized in Sec. III.

1. EXPERIMENTAL SETUP

HL-3 tokamak realized its first plasma in December 2020, whose missions are to support the operation of ITER and the design of future fusion devices in terms of the technological and physical facets [17]. The HL-3 tokamak has a D-shaped poloidal cross-section, whose original aspect ratio is R/a = 1.78/0.65 and maximum elongation reaches 1.8. The machine operates with toroidal fields of up to 2.5 T and has reached high plasma currents of 1.6 MA in diverter experiments. HL-3 tokamak is now equipped with 5 MW NBI with two tangential beamlines, 5 MW (at 105 GHz) and 0.5 MW (at 68 GHz) electron cyclotron resonance heating (ECRH) together with 2 MW LHCD at 3.7 GHz. The improved confinements such as the internal transport barrier (ITB) configurations and external transport barrier or H-modes have been realized. The first wall is fabricated with graphite tiles which are designed to take the high power loading from plasmas.

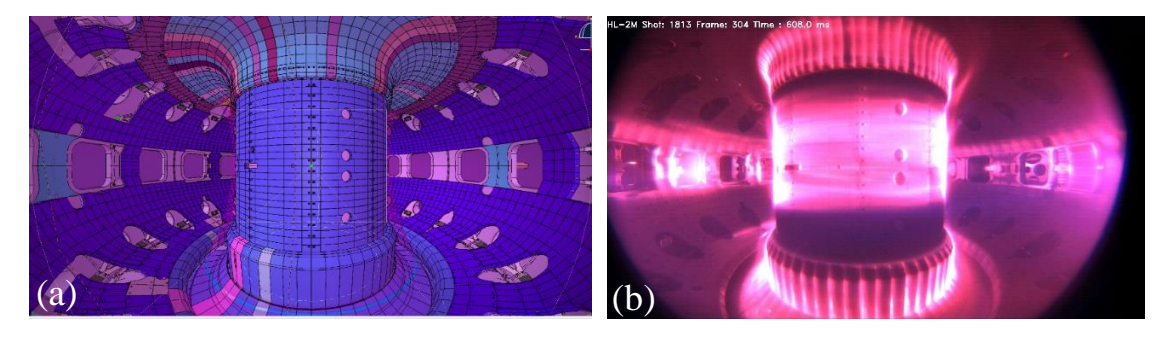


Fig. 1. (a) The modeled FOV by CATIA, and (b) real FOV obtained by the imaging system during a serious PWI event.

As shown in Fig. 1(a), a picture generated with the mechanical design software (CATIA) represents an inner scene of the machine vessel, using the view originating from #19 sector where the virtual camera is located. The wide-angle view allows the observation of various regions inside the torus, including the divertor, the inner and outer walls as well as the LHCD antenna and NBI port. The real imaging system, located in an equatorial port on #19 sector, consists of a front-end ultrawide-angle imaging lens that produces an intermediate image, three groups of bilateral telecentric relay lenses, and a color camera with a frame rate of up to 2000 frames per second (fps). This alignment approach allowed to be long transmitted distance (≥2 m) of the image is for reducing a radiation effect such as high neutron load on the detector. It optical structure is analogous to the extreme wide-angle view diagnostic in Ref. [18]. This imaging system gives us a FOV of 120 °(H) x 70 °(V) with a 1920×1080 CMOS pixel detector (pixel size of 10 um), as shown during a serious PWI event in Fig. 1(b). A spatial resolution of ~ 5 mm at an object distance of 3.5 m is achieved by this system. As can be seen, the modeled FOV [Fig. 1(a)] and real FOV [Fig. 1(b)] agree well with each other.

Here is the description of emission spectroscopy system for the studies of fuel recycling, first wall erosion, and impurity influx on the HL-3 tokamak. The horizontal chords view the inner wall, and vertical chords view the wall regions at the low field side, as indicated in Ref. [18]. Several individual lines of sight observe the divertor emission spectroscopy. A visible bremsstrahlung array at the poloidal cross-section is for the $Z_{\rm eff}$ measurement.

2. EXPERIMENTAL RESULTS

2.1. Hot spots distribution

The hot spots are static regions of the vacuum vessel reaching high temperatures due to concentrated plasma—wall interactions. The hot spots arise from one or more of the reasons: disruption damage, misaligned tiles, field ripple, and limiter/divertor tile design. The large FOV of visible observation allows gaining information on the spatial distribution of hot areas on the walls by observing the shining areas during a discharge. In a discharge of upper null divertor configuration, a bright hot spot is created at the junction of vertical tile and horizontal tile in the divertor, plus some continuous hot spots exist on the upper baffle, as shown in Fig. 2(a). The hot spot positions are quite localized and co-incident with the strike points as shown by the EFIT configuration in Fig. 2(b). The hot spots distribution causes the impurity influxes increase. The carbon influxes are deduced from the CIII emission taking into account the plasma edge parameters (density, electron temperature, Mach number) by using codes.

In HL-3 tokamak, the deviations from toroidal symmetry of the graphite tiles which forms the wall surface cause hot spots which preferentially intercepts the power influx in the scrape-off layer. The power handling of the wall is then constrained by localized heating of these spots, rather than by the toroidally averaged power flux in the SOL. To increase the power-handling capability of the inner wall, the tile alignment should be improved, so that deviation from toroidal symmetry are only ± 0.5 mm.



FIG. 2. (a) Hot spots distribution on the wall and (b) EFIT configuration at 1556 ms of Shot 5054.

2.2. Dusts motion and magnetic field lines development

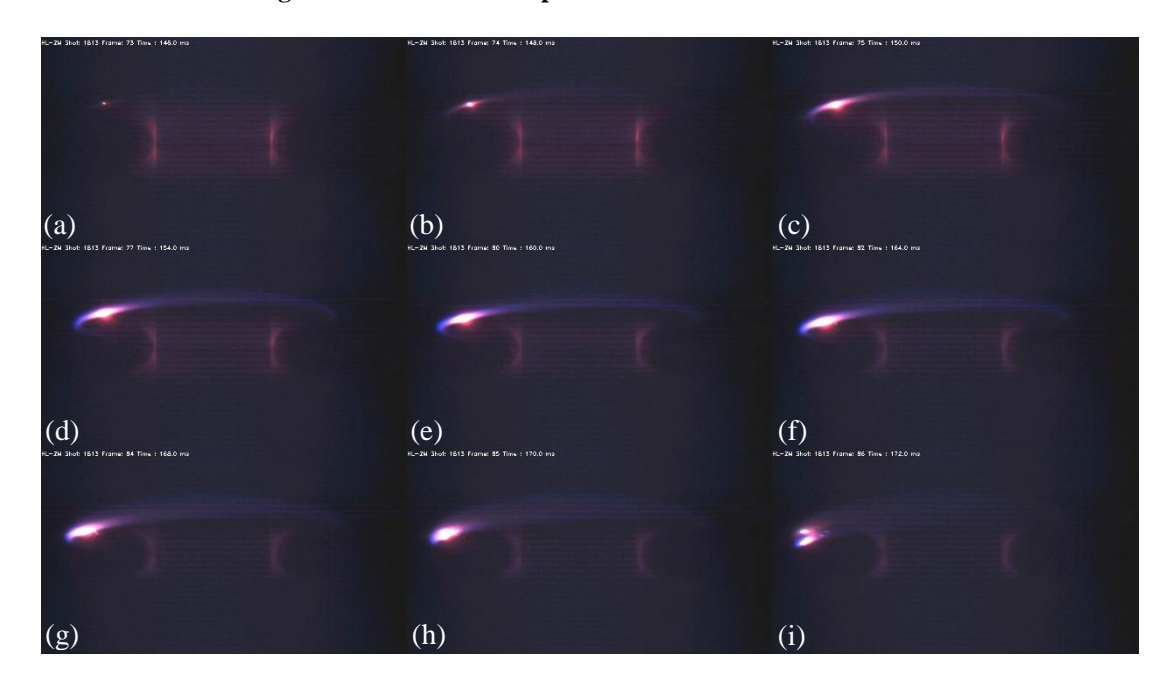


FIG. 3. Dusts motion evolution in plasma edge and magnetic field lines development in Shot 1813.

The high resolution of the imaging system allows the disclosure of many details of dusts evolution. In video images of Shot 1813, the UFO appears as bright small dust particle [Fig. 3(a)] at 146 ms and then moves fast at the plasma edge [Fig. 3(b)- Fig. 3(h)], and finally it is divisive and ejected by the plasma [Fig. 3(i)]. During its movement at the plasma edge, it is ablated and shines along the magnetic field lines, accompanied by the magnetic field lines development mainly because of the low charge-state impurity ions diffuse along the magnetic field lines.

For the dusts generation, the first type is small dust particles which are remaining in the vessel after the long-term in-vessel work. The second type of impurity events is caused by the material release due to the direct plasma-wall contact. During normal HL-3 plasma operation, the released material is mainly carbon. However, in case of technical and physics problems such as loss of plasma position control, electrical problems or overheating of invessel components, also other materials apart from carbon may come into contact with the discharge and may reach significant concentrations in the plasma and result in major disruption.

2.3. Boron powder injection

In Shot 6618, the online boron powder injection from the top of vacuum vessel beginning at 540 ms is implemented in order to improve the wall condition and study the boron transport behaviours, where the interactions between the plasma edge and puffed boron powders are observed, as shown in Fig. 4(f). The boron powder gathers and shines in the plasma edge, which is probably by the impurity screening mechanism. Almost simultaneously, the visible radiation (mainly the bremsstrahlung) enhancement in the plasma center because of the impurity pollution occurs, as shown in Fig. 4(c). Actually, a low recycling level indicated by D α radiation (black line) and low carbon influx indicated by the CIII 464.7 nm radiation (red line) between 550 ms to 800 ms as shown in Fig. 4(d), as well as a high confinement phase indicated by the shaded area is concurrently achieved by the online boron powder injection. Z_{eff} during the high confinement phase is continuously increased, as shown in Fig. 4(e).

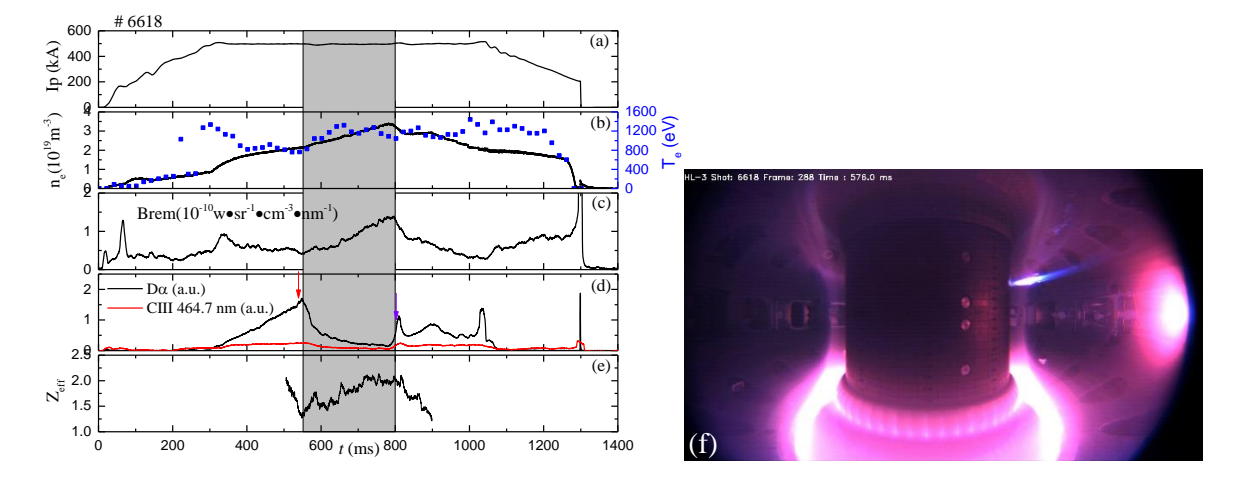


FIG. 4. Time evolution of plasma parameters of (a) plasma current Ip, (b) central electron temperature T_e and line-averaged electron density n_e, (c) visible bremsstrahlung intensity, (d) divertor Dα radiation (black line) and CIII 464.7 nm radiation (red line), and (e) Z_{eff} for Shot 6618. The red and purple arrows in Fig. 4(d) represent the beginning time and end time of the boron powder injection. Fig. 4(f) shows the interaction image of the injected boron powder and plasma edge.

2.4. Disruption

Transient events such as disruptions produce large heat flux to the wall in a short time which may induce unacceptable erosion due to melting and sublimation of the materials. A major disruption is the most dangerous form of tokamak instability. HL-3 plasmas have vertically elongated cross section making their vertical position unstable. Virtually most disruptions in HL-3 tokamak are either caused by, or result in fast vertical displacement of the plasma, eventually terminating in contact with internal hardware at the top or bottom of the vacuum vessel.

The progress of plasma breakdown is recorded by the high-speed camera and the time resolution (500 fps) being sufficient to resolve disruption. Figure 5 displays the plasma disruption evolution in Shot 5091. The pre-disruption configuration is lower single null with the strike points in the corners of the divertor, as shown by the plasma image in 2002 ms in Fig. 5(a). Firstly, in vertical displacement events (VDE's) the control of the plasma vertical

position is lost prior to disruption. This results in a fast transition between limiter and divertor plasmas at the moment the plasma actually disrupts, as shown by the plasma images in Fig. 5(b) - Fig. 5(d) from 2152 ms to 2178 ms. Secondly, during the plasma current decay, stored magnetic energy is radiated over the whole vessel, as shown by such a high level of plasma light in Fig. 5(e). It appears that magnetic energy has contributed to the energy conducted to the walls. It is reasonable to expect that contact with the walls during the current decay would result in some wall heating. Finally, the position control is lost, and the plasma moves vertically up while simultaneously shrinking in cross section, as shown in Fig. 5(f). During collision with the top or bottom of the vessel, currents flow through the vacuum vessel resulting in large forces. The current quench is followed within a few tens of milliseconds. The process of so called plasma 'soft-land' during current decay in Shot 5090 is shown in Fig. 6. As can be seen, the standard divertor configuration [Fig. 6(a)] is then translated to the limiter configuration [Fig. 6(b) and Fig. 6(c)], accompanied by the plasma cross section shrinking. Finally, the plasma is extinguished on the inner wall, as shown in Fig. 6(d). Figure 7 shows the current decay in Shot 5090 (red line) and Shot 5091 (black line), respectively.

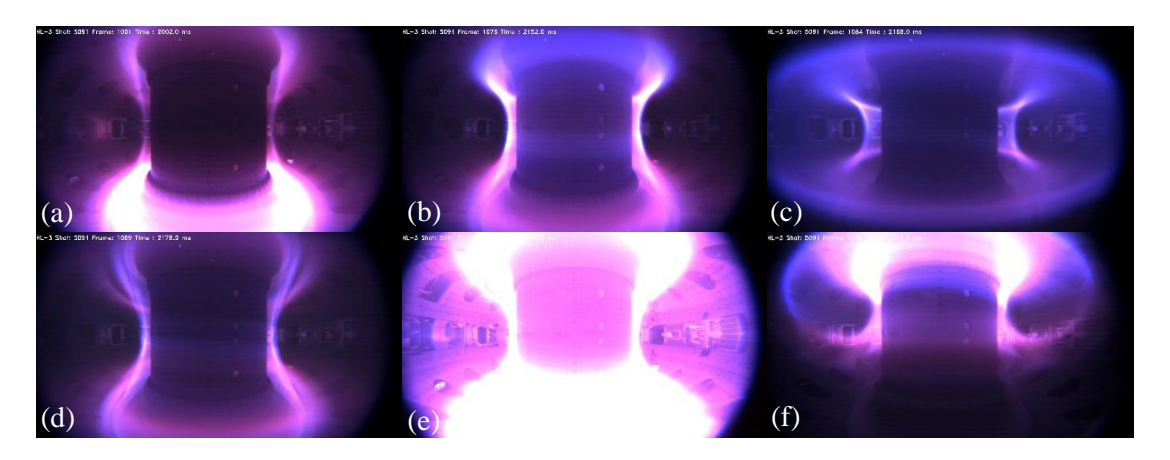


FIG. 5. Visible images of the plasma disruption evolution in Shot 5091.

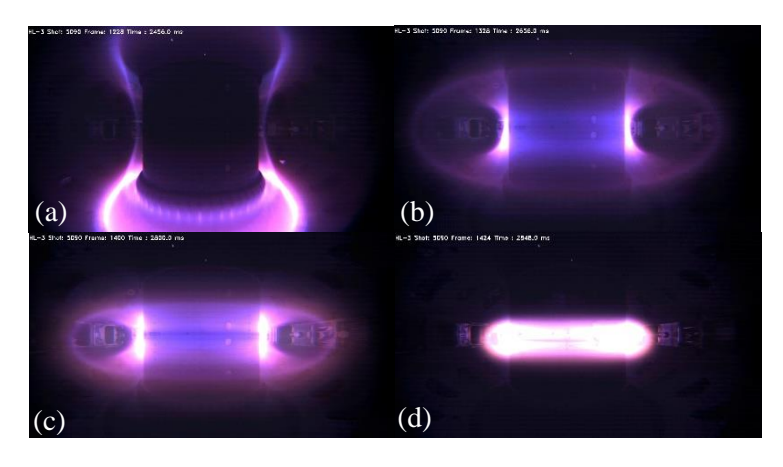


FIG. 6. Visible images of the plasma 'soft-land' in a controlled positon in Shot 5090.

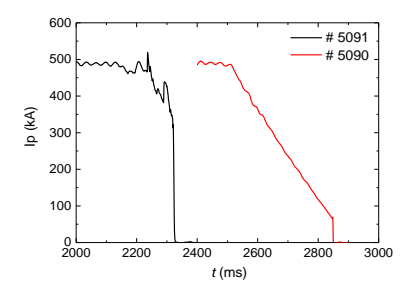


FIG. 7. The current decay in Shot 5090 (red line) and Shot 5091 (black line).

2.5. ELmys

The edge plasma pressure increase caused by the formation of an ETB does not occur usually in a stationary way but experiences quasi-periodic relaxations, which are called ELMs. ELMs can be classified into three types (I, II and III) depending on their frequency dependence on input power and pedestal plasma pressure. Although the total plasma energy loss caused by ELMs is relatively small, the associated energy fluxes on PFCs can be very large and lead to large temperature increases at the PFC surface. This is due to the short time scale over which this loss takes place and to the relatively small area on the divertor on which this power flux is deposited.

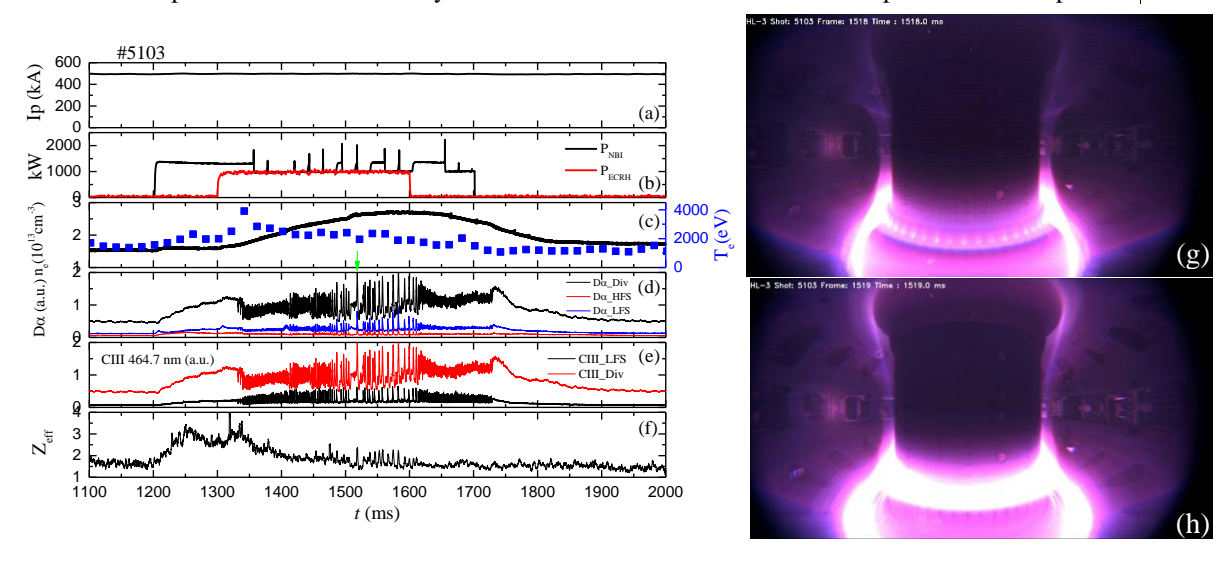


FIG. 8. Time evolution of the deuterium recycling [Fig. 8(d)] and CIII carbon influx [Fig. 8(e)] on the divertor, and wall at the low field side in Shot 5103. Figure 8(g) and Fig. 8(h) present the lumeneous difference obtained from two consecutives frames. The camera acquisition frequency is 1000 fps.

The PWI is studied in ELMy H-mode discharge in a lower single null configuration in HL-3 tokamak. Detection of ELM Bursts and L-H D α step occurs using the fast camera with acquisition frequency of 1000 fps. Figure 8(g) and Fig. 8(h) present the lumeneous difference obtained from two consecutives frames in Shot 5103: one before the ELM at 1519 ms, one during the ELM at 1520 ms. It shows that the plasma wall interactions are not only localized in the divertor, during ELMs, but a part of the ELMs energy is also deposited on the upper limiter. Almost no interaction is observed on the inner and outer walls during ELMs. They are consistent with the emission spectroscopy measurements and the recycling properties have been studied extensively. The measured emission spectroscopy during an ELM cycle shows enhanced deuterium recycling and CIII carbon influx during the deposition of the ELM particle pulse at the divertor target, as shown in Fig. 8(d) and (e) respectively. Nevertheless, the midplane recycling shows a relatively low level.

As shown in Fig. 8(f), $Z_{\rm eff}$ during one ELM event is increased, indicating the transiently increased impurity influx because of PWI. Nonetheless, $Z_{\rm eff}$ is basically decreased during the H mode period, which demonstrates the impurities are expelled from the plasma by the type-I ELMs. The more the ELMs frequency is, the more impurity is expelled from the plasma. $Z_{\rm eff}$ behavior can be explained by this: contrary to normal divertor operation, the impurity screening of the divertor during ELMs is quite poor and, hence, the probability that a significant part of these atoms reaches the main plasma is high. This is due to the existence of a strong particle outflux from the divertor following the ELMs, caused by to the bouncing back (along the field lines) of the pressure increase due to the ELMs at the divertor target, which occurs simultaneously with the arrival of the ELM energy flux at the divertor. This large carbon influx will lead to a large increase of the $Z_{\rm eff}$ and a large dilution at the plasma edge. Whether this will lead to a large increase of the $Z_{\rm eff}$ at the core plasma and to the termination of the high fusion production regime depends on the relative timescales of the inwards diffusion of these impurities towards the core and the ELM repetition time. ELMs are very effective in flushing out impurities, as the plasma particles expelled by the ELM come from the pedestal region where the concentration of impurities is highest.

3. SUMMARY

PWIs are not only concentrated in the divertor region, but also on the main chamber which may occur in case of ELMs, disruptions, etc. The visible lines are emitted primarily from atoms and ions with low ionization, therefore, these lines are often used to monitor particle influxes in the plasma edge or wall erosion rates, as well as the interaction between the plasma edge and the wall. An ultra-wide angle view in the visible range whose objective is to monitor the main chamber and divertor and to insure routine PFC protection, is installed on HL-3 tokamak. The hot spots distributions and dusts movements have been captured by the high resolution cameras. The first results on the plasma wall interaction during disruption and ELMs have been recently obtained during the HL-3 operations.

ACKNOWLEDGEMENTS

This work was supported in part by the National Key Research and Development Program of China under Grant 2022YFE03180200 and Grant 2019YFE03010004, in part by the National Natural Science Foundation of China under Grant 12275070, Grant 12205084, and Grant 12105085.

REFERENCES

- [1] R. Neu, M. Balden, V. Bobkov, et al. "Plasma wall interaction and its implication in an all tungsten divertor tokamak," Plasma Phys. Control. Fusion 49 (2007) B59–B70.
- [2] A.J.H. Donne, A.E. Costley, R. Barnsley, et al. "Chapter 7: Diagnostics," Nucl. Fusion 47 (2007) S337–S384.
- [3] M. Ulrickson, the JET Team and The TFTR team, "A review of carbon blooms on JET and TFTR," J. Nucl. Mater. 176 & 177 (1990) 44-50.
- [4] P. Andrew, A. Alonzo, G. Arnoux, et al. "First measurements of main chamber power load during JET disruptions," J. Nucl. Mater. 363–365 (2007) 1006–1010.
- [5] E. Gauthier, P. Andrew, G. Arnoux, et al. "Plasma wall interaction during ELMs in JET," J. Nucl. Mater. 363 365 (2007) 1026 1031.
- [6] R.A. Pitts, P. Andrew, G. Arnoux, et al. "ELM transport in the JET scrape-off layer," Nucl. Fusion 47 (2007) 1437–1448.
- [7] E. Gauthier, "Progress in diagnostics for characterization of plasma wall interaction in tokamaks," J. Nucl. Mater. 390–391 (2009) 1059–1065.
- [8] A. Loarte, "Implications of the use of Carbon-Based Plasma Facing Components in Next Step Fusion Devices," Physica Scripta. Vol. T111 (2004) 13–22.
- [9] I. Balboa, E. Rose, G.F. Matthews, et al. "Remote wide angle view broad wavelength viewing system compatible with D-T operations in JET," Plasma Phys. Control. Fusion 65 (2023) 064005.
- [10] I. Balboa, E. Rose, G.F. Matthews, et al. "Remote infrared view of JET divertor compatible with D-T operations," Plasma Phys. Control. Fusion 65 (2023) 094002.
- [11] D. Guilhem, J.L. Bondil, B. Bertrand, et al. "Tore-Supra infrared thermography system, a real steady-state diagnostic, Fusion Eng. Des. 74 (2005) 879–883.
- [12] J. Cantarini, D. Hildebrandt, R. König, et al. "Optical design study of an infrared visible viewing system for Wendelstein 7-X divertor observation and control," Rev. Sci. Instrum. 79 (2008) 10F513.
- [13] A.N. James, D. Brunner, B. Labombard, et al. "Imaging of molybdenum erosion and thermography at visible wavelengths in Alcator C-Mod ICRH and LHCD discharges," Plasma Phys. Control. Fusion **55** (2013) 125010.
- [14] K. Kamiya, K. Itami, M. Takeuchi, A. Enokuchi, "Design study of a wide-angle infrared thermography and visible observation diagnostic on JT-60SA," Fusion Eng. Des. 89 (2014) 3089–3094.
- [15] P. Andrew, A. Alonzo, G. Arnoux, et al. "First measurements of main chamber power load during JET disruptions." J. Nucl. Mater. 363-365. (2007) 1006-1010.
- [16] T. Craciunescu, A. Murari, M. Gelfusa, et al. "Overview of image processing tools to extract physical information from JET videos," Plasma Phys. Control. Fusion 56 (2014) 114006.
- [17] L. Liu, X.F. He, D.L. Yu, et al. "Visible wide-angle view imaging system for the first plasma on the HL-2M tokamak," Appl. Opt. 60 (2021) 3211-3216.
- [18] L. Liu, F. Xia, Z.W. Chen, et al. "Multi-directional observations of the high-performance plasmas by visible imaging diagnostics on the HL-2M tokamak", IEEE Trans. Plasma Sci., 52 (2024) 1328-1336.